Click chemistry binding of colloidal quantum dots and gold nanoparticles revealed by combined confocal DLS and FCS

Pierre Bauer, Ali Dabbous, Sébastien Pairis, Vincent Maurel, Fabien Dubois, Aude Barbara

Click chemistry binding of colloidal quantum dots and gold nanoparticles revealed by combined confocal DLS and FCS

Pierre Bauer,[†] Ali Dabbous,[‡] Sébastien Pairis,[†] Vincent Maurel,[‡] Fabien Dubois,[†] and Aude Barbara[*,†]

[†]*Université Grenoble Alpes, CNRS, Grenoble INP, Institut Néel, 38000 Grenoble, France*

[‡]*Université Grenoble Alpes, CEA, CNRS, Grenoble INP, IRIG-SyMMES, 38000 Grenoble, France*

E-mail: aude.barbara@neel.cnrs.fr

Abstract

Click chemistry reactions were employed to synthesize hybrid systems consisting in CdSe-ZnS quantum dots (QDs) and gold nanoparticles (AuNPs). These colloidal systems were characterized by an experimental approach of combined confocal dynamic light scattering and fluorescence correlation spectroscopy which we developed to independently study the hydrodynamic properties of the QDs and those of the AuNPs. We demonstrate that this method allows to unambiguously reveal the particles binding, even in cases where this issue cannot be ascertained by common experimental approaches. Furthermore, we determined the nature of the formed hybrid systems using a hydrodynamic bead model approach, and characterized the efficiency of the reaction process. None of these results are accessible through other characterization methods and they pave the way for a more quantitative understanding of the physicochemical properties of such hybrid systems.

Keywords:

Introduction

Hybrid systems composed of metal nanoparticles (NPs) interacting with quantum dots (QDs) have gained increased interest over the last decades as they appear as promising candidates for improving and better controlling photochemistry or photoelectronic properties at the nanoscale level.[1] The underlying idea is to form exciton-plasmon near-field interactions which will allow charge and energy transfers, thereby redefining the optical and electronic properties of the individual components.[2–5] The fields in which these hybrid systems are studied are quite wide, ranging, from quantum plasmonics,[6,7] to non-linear optics[8,9] or catalysis.[10,11] Various elaboration processes have been investigated to obtain QD-NP hybrid materials which include the growth of metallic shells on QDs,[12] that of semiconductors on metal NPs[13] or the selective deposition of QDs on plasmonic structures.[14–16] A different approach is to form self-assembled systems of colloidal QDs and colloidal metal NPs where the particles are connected via electrostatic interactions[17] or via bio-bounding through DNA[18,19] or artificial proteins.[20] The use of colloids is appealing due to robust and readily accessible preparation routes, both for the metal NPs[21–23] and for the QDs.[24] Additionally, they enable tunable optical and electronic properties of the initial particles which highly depend on the size and shape of the latter.[24–28] Finally, the distance separating NPs and QDs which is a key factor in their near-field coupling,[1,4,29,30] may be adjusted through the length of the bridging species.[31] Considerable versatility is thus achievable, however, it often comes with the drawback of limited control over the synthesized objects. Thus, the quantitative understanding of the physical properties of the as-formed hybrid systems necessitates access to reliable characterization techniques.

In most reported studies, the characterization of colloidal hybrid systems is supported by Transmission and Scanning Electron Microscopy (TEM/SEM), UV-Visible extinction and

static or time-resolved photoluminescence measurements. Electronic microscopy gives robust indications on the morphology of the particles but probes a limited number of particles and the preparation of the liquid samples which involves a drying process, can alter the colloidal state of the particles. Optical spectroscopies offer appreciable complements to SEM/TEM as they are non-destructive and *in-situ* approaches, and they probe a more significant part of the sample. Yet, UV-visible extinction spectra are governed by the optical properties of the metal NPs whose scattering and absorption coefficients are several orders of magnitude higher than those of the QDs, in the visible range. As a result, the formation of metal NPs aggregates can be detected but without knowing whether they result from a colloidal instability or from the effective formation of hybrid systems containing QDs. Conversely, photoluminescence and lifetime measurements provide information on the QDs and their possible binding to metal NPs, as a non-radiative decay of the exciton in the metal is expected in this case. This effect is accompanied by a fluorescence quenching and a shortened time of the excited state.[32] However, quenching of QDs has also reported in mixtures of non-connected QDs and metal NPs.[33,34] Finally, none of these spectroscopies give a direct proof on the particles linking, nor any indications on the nature and the size of the formed hybrid objects.

Dynamic Light Scattering (DLS) is a technique widely used in colloidal science which offers a possibility of determining the size distribution of particles in suspension. However, when aggregates/hybrid systems form, and particularly if they deviate significantly from a spherical shape, or at high heterogeneity levels, the technique provides an average size value that poorly reflects the actual nature of the objects in suspension. Moreover, QDs are difficult to characterize by DLS as they are very weak scatterers. The latter can however be studied by Fluorescence Correlation Spectroscopy (FCS), to access their size or their blinking properties.[35–37] Hence, these experiments appear to have a potential to be further explored and to offer insights that are not accessible through other characterization methods. Yet they are not reported within the framework of hybrid systems.

In the present paper, we propose a novel experimental approach of combined confocal DLS and FCS to investigate the colloidal state of hybrid systems. The systems studied are CdSe-ZnS core-shell QDs linked to gold NPs (AuNPs) by a Copper-Catalyzed Azide to Alkyne Cycloaddition (CuAAC) reaction,[38] commonly referred to as "click reaction", and that were reported by our group as potential photocatalysts.[11]This click reaction involves the formation of triazole groups through a Huisgen 1,3-dipolar cycloaddition of organic azides and alkynes.[39] Initially developed as an efficient approach to develop new strategies for gold nanoparticles functionalization,[40] it offers high specificity, effectiveness in water at low concentration, and enables the grafting of a large number of functional ligands or biomolecules onto particle surfaces.[41] It has also been demonstrated to be pertinent in colorimetric sensing of copper ions in aqueous solution.[42] However, to our knowledge, click chemistry is seldom utilized to prepare composite hybrid systems between two different types of particles (metal, semiconductor, etc.), covalently attached via the formation of a triazole ring.[43] In this study, we used two synthesis routes based on the click chemistry approach : (i) a selective click reaction dedicated to specifically form AuNP-QD bonds, thereby optimizing the formation of hybrid systems, and (ii) a non-selective click reaction, where the binding can occur between any type of particles but that forms shorter and more favorable to electron delocalization bonds, thereby enabling a better coupling between the particles (Fig.1). The systems were characterized by combined confocal DLS and FCS to specifically and independently investigate the colloidal state of both the AuNPs and that of the QDs. The combination of DLS and FCS permits the merging of information on the aggregation state of the AuNPs obtained from DLS and that of the QDs obtained by FCS, thus characterizing the hybrid systems. Additionally, the confocal approach provides access to the fluctuations of the local concentration of the particles and enables a better characterization of the heterogeneity and the nature of the formed aggregates. As will be presented, a more thorough and quantitative characterization of the hybrid system was obtained as compared to standard characterization means. In particular, the validation of the click process was unambiguously assessed. The

efficiency of the reaction was also assessed by distinguishing different situations where (i) the NPs and the QDs are not connected,(ii) hybrid QDs-NPs systems are formed and co-exist with remaining non-connected particles or (iii) hybrid systems are massively formed. Finally, the nature of the formed hybrid systems was identified using the appropriate hydrodynamic models.

Confocal DLS and FCS Theoretical Background

Normalized Auto-Correlation Functions in DLS and FCS

DLS and FCS belong to the class of photon correlation spectroscopy experiments by which the translational diffusion coefficients D of colloidal NPs can be measured. The general underlying principle is that the measured intensity, Rayleigh scattering for DLS or fluorescence for FCS, fluctuates as a function of time due to the motion of the particles. These fluctuations can be statistically analyzed to characterize the dynamics of the system, by deriving the normalized intensity auto-correlation function (ACF):

$$G(\tau) = \frac{\langle I(t)I(t+\tau)\rangle}{\langle I(t)\rangle^2},$$

where $\langle ...\rangle = \lim_{T\to\infty} \frac{1}{T}\int_0^T ...dt$ is an integration over the acquisition time.

Considering freely diffusing spherical NPs, i.e non-interacting particles driven by a Brownian motion, and a confocal volume where the laser intensity distribution can be described by a 3D-Gaussian law $I(x,y,z) = I_0 e^{-2(x^2+y^2)/r_0^2 - 2z^2/z_0^2}$, the DLS ACF writes as:[44]

$$G(\tau) - 1 = \beta e^{-2\tau/\tau_c} + \frac{c^2}{\langle N\rangle}\frac{1}{(1+\tau/\tau_D)(1+\tau/w^2\tau_D)^{1/2}}. \quad (1)$$

The first term is the so-called interference term, due to the interferences of the electric fields scattered by the different NPs.[45] This term decays with a characteristic time $\tau_c =$

$1/2q^2D$, where $q = 4\pi n \sin(\theta/2)/\lambda$ is the scattering vector, θ being the scattering angle, n the refractive index of the solvent, λ the laser wavelength, and D is the translational diffusion coefficient of the NPs. β is an adjustable parameter[45] related to the experimental setup, with $0 \leq \beta \leq 1$.

The second term, referred as the number fluctuations term, models the variation as a function of time of the local concentration in the observation volume.[46] It decays with a characteristic time $\tau_D = r_0^2/4D$ where D is also the translational diffusion coefficient of the NPs, as in the first term. Finally, $\langle N \rangle$ is the average number of NPs in the observation volume, c is the ratio of the signal from the NP to the total measured intensity[47] and $w = z_0/r_0$.

In standard DLS, the interference term dominates as the probing volume, typically a few mm^3, samples a large number of NPs and the term $1/\langle N \rangle$ tends to zero. Only in rare situations of extremely diluted samples can the second term become significant,[44,46,48] however the signal to noise ratio is then noticeably deteriorated and the measurement times are long.

Regarding FCS experiments, only the variation of the local concentration gives rise to intensities fluctuations as fluorescence is not a coherent process. The expression of the ACF is then given by Eq. (1) without the interference term i.e according to:

$$G(\tau) - 1 = \frac{c^2}{\langle N \rangle} \frac{1}{(1 + \tau/\tau_D)(1 + \tau/(w^2\tau_D)^{1/2}}. \tag{2}$$

To improve the signal to noise ratio and shorten the measurements times, Rigler et al.[49] proposed to carry out the experiments under a confocal microscope to reduce drastically the probing volume to $\sim 1\mu m^3$. The number of NPs present in the observation confocal volume is consequently reduced thereby enabling to increase the fluctuation amplitudes at unchanged concentrations and hence to improve the signal-to-background ratio. Another advantage of the small confocal volume is that it shortens the translational correlation time. Following these FCS experimental conditions, DLS measurements using a confocal configuration have

also been carried out. The latter permits the characterization of more concentrated colloidal suspensions, a higher accuracy of the diffusion vector[50,51] and, as we will see below, a better analysis of the size dispersion of the NPs in solution.

Hydrodynamic diameters determination

In the present study, and as it is very often the case, the translational diffusion coefficient D is experimentally determined to access the hydrodynamic diameter d_H of the NPs. When the latter are spherical, this is easily realized by applying the Stokes-Einstein relationship:[52]

$$d_H = \frac{k_B T}{3\pi\eta D},$$

where T and η are the temperature and the viscosity of the solvent respectively and k_B is the Boltzmann constant. The hydrodynamic diameter then corresponds to a slightly increased value of the physical diameter, due to the molecules surrounding the particles in solution. The assumption of sphericity will be here perfectly justified when dealing with the colloidal solutions of the primary AuNPs and that of the QDs. However, the study of aggregates or hybrid objects requires the use of more realistic, but also more sophisticated, hydrodynamic models considering chain-like[53,54] or fractal[55] aggregates of spherical primary particles. In these models, the diffusion coefficient of an aggregate $D_A = \frac{k_B T}{3\pi\eta d_A}$, where d_A is its apparent hydrodynamic diameter, is defined as:

$$D_A = \alpha D_{eq},$$

where $D_{eq} = \frac{k_B T}{3\pi\eta d_{eq}}$ is the diffusion coefficient of a sphere of a volume equivalent to that of the aggregate or the hybrid system under consideration, d_{eq} being its equivalent diameter. The value of α is accessed numerically and depends on the number of primary particles and on the fractal dimension of the agregate.

In the present case, we used the chain-like (or bead) model of linear aggregates, which was shown to be relevant in the context of chemical bonding between spherical particles.[56] For aggregates formed by n_s identical spheres of diameter d_0 , the apparent diameter then writes as:

$$d_A = \frac{d_{eq}(n_s)}{\alpha(n_s)}, \tag{3}$$

with $d_{eq}(n_s) = d_0\sqrt[3]{n_s}$ and where the values of $\alpha(n_s)$ are taken from Ref.[53,54] Considering hybrid systems, a more realistic model involves linear aggregates formed by a combination of n_s primary spheres of two different sizes d_0 and d_1. Eq.3 is then applied with an equivalent diameter $d_{eq}(n_s, n) = d_0\sqrt[3]{n + (n_s - n)\left(\frac{d_1}{d_0}\right)^3}$, n being the number of spheres of diameter d_0. It is worth noting that in reality, the values of $\alpha(n_s)$ vary depending on whether the aggregates contain only identical spheres or not. However, in the latter case, the values of $\alpha(n_s)$ were not found in the literature, except for asymmetric dimers.[54] Nevertheless, the discrepancy between the two dimer models leads to differences in the determination of d_A which are small compared to the accuracy of the experiments, thus justifying our approximation.

Chemicals and Materials

Chemicals. D-histidine, sodium hydroxide, chloroform, methanol, ethanol, sodium tetraborate decahydrate (ACS reagent > 99%), sodium citrate tribasic dihydrate (ACS reagent > 99%), hydrogen tetrachloroaurate trihydrate (≥ 99%), sodium-L-ascorbate (≥ 98%), amino-PEG_8-acid (≥ 90%), 3-Azido-1-propanamine (≥ 95%), 1,4-Diethynilbenzene ($C_{10}H_6$, ≥ 96%), were purchased from Sigma-Aldrich. Copper sulfate pentahydrate (≥ 98%) was purchased from Alfa Aesar. Propargyl-PEG_9-amine (≥ 95%) was purchased from BroadPharm. All reactants were used without any further purification. 4-Azidobenzyl phosphonic acid was synthesized following the procedure reported by Schönweiz et al.[57]

Quantum Dots. Core-Shell CdSe/ZnS QD with a core of 4 nm and a total diameter of 10

nm, in suspension in toluene and coated with octadecylamine ligands were purchased from NN-Labs Laboratories.

Filters. Minisart® NML syringe filters with surfactant-free cellulose acetate (SFCA) membranes and pore sizes of 0.45 μm were purchased from Sartorius and were used during the functionnalization of the gold particles. Vivaspin® 2 concentrators with 100 kDa MWCO pore size polyethersulfone (PES) membranes and 30 kDa centrifugal filters (Millipore Amicon) were purchased from Sigma.

Starting Particles

Gold Nanoparticles Spherical citrate-capped gold nanoparticles (AuNPs) were first prepared following the classical method of reduction of tetrachloroauric acid ($HAuCl_4$) with trisodium citrate (Na_3Cit) in an aqueous medium at 100°C.[22,23] Here, the ratio $Na_3Cit/HAuCl_4$=2.4 was kept constant while the initial quantity of $HAuCl_4$ was 0.32 mmol for the AuNPs used in the non-selective click reaction and 0.160 mmol for the AuNPs used in the selective click reaction.

CdSe/ZnS core-shell Quantum Dots To make the commercial CdSe/ZnS suitable for the CuAAC reactions, a transfer from their native toluene solvent to an aqueous solution was required. The latter is based on a procedure reported in Ref.[58] and was detailed elsewhere.[11] Briefly, QDs suspended in toluene are dried and re-dispersed in chloroform. After addition of a 3:1 methanol:basic water solution of histidine, a phase separation occurs between the organic solvent and the water containing the QDs. The complete colloidal stabilisation of the quantum dots in the aqueous phase was then obtained by addition of histidine solubilized in basic water. The final suspension was washed several times with chloroform, filtered with a 30-kDa Amicon centrifugal filter and finally re-dispersed in a pH=10 borax buffer solution. The final concentration of the QDs suspension was determined by UV-visible extinction measurements and using the molar extinction coefficients reported by Jasieniak et al.[59]

Selective Click Reaction Procedure

In order to target specifically the formation of AuNP-QD bonds, a selective click reaction, that can only occur between AuNPs and QDs, was used. The latter is based on the bonding of alkyne-tagged AuNPs to azide-tagged QDs via the azide-alkyne CuAAC reaction, as schemed in Fig.1. According to Marti el al.,[60] a key factor in the success of such a reaction is the stabilization of the functionnalized AuNPs before using them for the click reaction. Consequently, the AuNPs were functionalized with a 1:1 molar equivalent mixture of short-length chains amino-PEG-alkyne and amino-PEG-COOH, the presence of terminal carboxylic acids being intended to ensure the stabilization of the surface charge density of the metallic nanoparticles.[60] In practice, 5 mL of citrate-capped AuNPs were mixed with a 15μL/15μL aqueous solution of propargyl-PEG_9-amine/amino-PEG_8-acid at 0.125 mM together with 10 μL of aqueous NaOH at 10 mM. The mixture was stirred overnight. The suspensions obtained were used without any other purification steps, except for a filtering at 0.45 μm before use. The azide-tagged QDs were obtained by mixing 50 μL of the aqueous suspension of histidine-capped QDs to 100 μL of a 5 mM (4-azidobenzyl) phosphonic acid ligands and 100 μL of 5 mM histidine both in a buffer solution. The sample was left 2 days at room temperature and was filtered twice, with a 30-kDa Amicon centrifugal filter, before use to eliminate any excess of ligands. The QDs were then re-dispersed in a borax buffer solution. Finally, the click reaction procedure, reported recently by our group,[11] consists in mixing AuNPs with 25 molar equivalent QDs and in adding sodium ascorbate:copper sulfate aqueous solution at 2:1 in concentration to catalyse the reaction.

Non-selective Click Reaction Procedure

The non-selective click reaction is based on the connection of azide-tagged AuNPs and azide-tagged QDs via a bridging bis-alkyne, here the 1,4-Diethynilbenzene (DEB). The azide-

alkyne CuAAC reaction can thus take place on both sides of the DEB, either with AuNPs or with QDs, thereby leading to the possible connection of AuNP-AuNP, QD-QD or AuNP-QD, as shown in Fig.1. The azide-tagged QDs were obtained in the same manner as for the selective click reaction, while the citrate-capped AuNPs were here functionnalized with 3-azido-1-propanamine (APA) using a process based on a ligand exchange developed by Hua et al.[61] Two mL of AuNPs at 6 nM were mixed with 60 μL of a 2 mM APA solution prepared in a 2:1 in volume ethanol:water solution. The mixture was immediately sonicated during 2 minutes and the azide-tagged AuNPs were obtained after 1 hour of reaction. The as-obtained azide-tagged AuNP were used without any other purification steps, except for a filtering at 0.45 μm before use, in order to minimize the possible formation of spontaneous aggregates. For the click reaction, 1 mL of water was mixed with 500μL of azide-tagged AuNPs. One point five mL of ethanol and 15 μL of 1.4 μM azide-tagged QDs were added and the sample was left undisturbed during 1 hour. Finally, 50 μL of a 0.3 mM DEB ethanol solution, 40 μL of a 0.1 mM sodium ascorbate 2:1 ethanol:water solution and 40 μL of a 0.05 mM copper sulfate water solution were added to induce the click reaction.

Reference Samples

For both types of click reactions (non-selective and selective), so-called reference samples were made. They consist of a mixture of supposedly non-connected AuNPs and QDs in the same chemical environment as in the samples prepared by click reaction (called hereafter clicked samples). In the case of the non-selective click reaction, the reference samples were obtained by carrying out the clicked reaction protocole without adding DEB. The reference samples of the selective click reaction were obtained by applying the click procedure using QDs bare of clickable ligands (QDs covered with histidine). In both cases, the reference samples were systematically characterized in parallel to the clicked samples in order to make

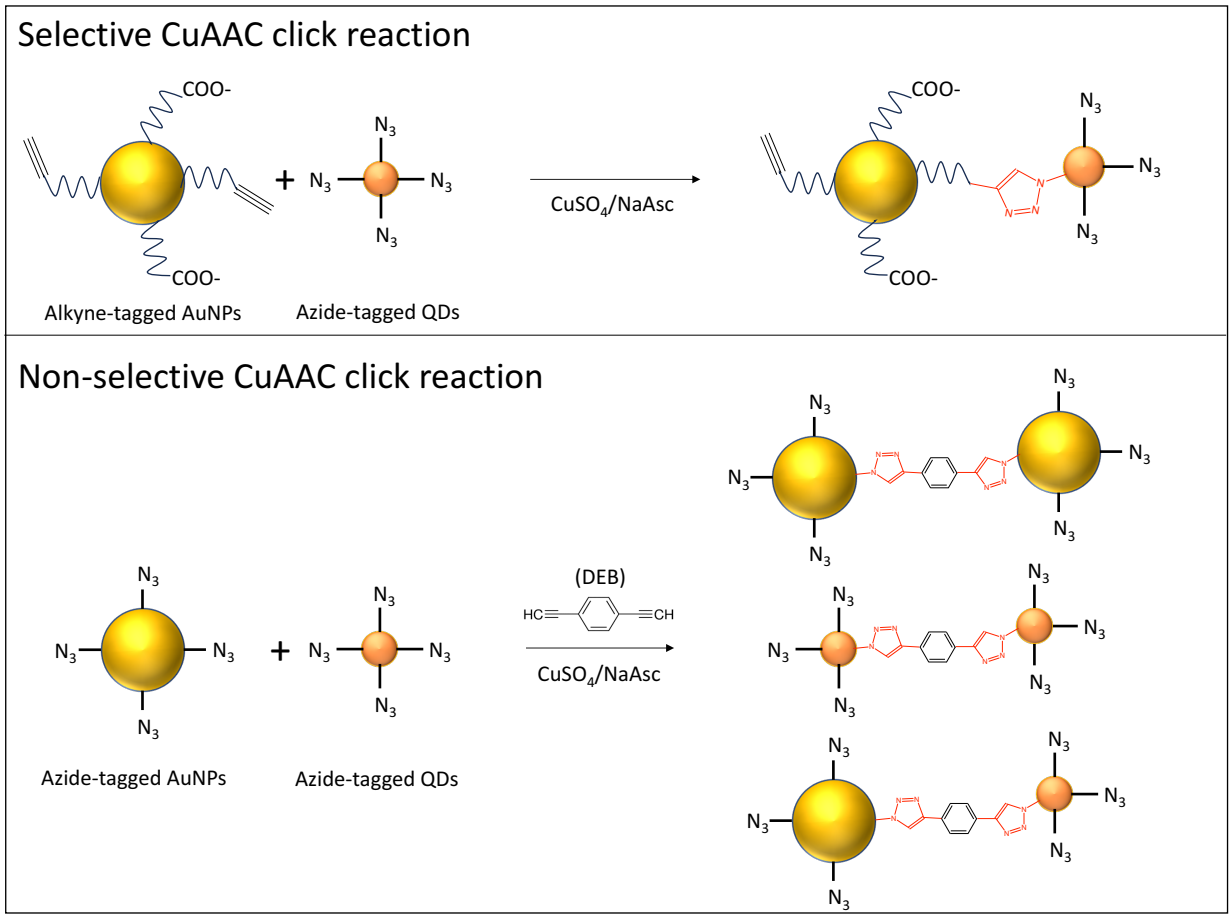

Figure 1: Schematic representation of the click reaction principle. (Upper pannel) Selective click where the azide-alkyne CuAAC click reaction is solely obtained between the alkyne-tagged AuNPs functionnalized with a mixture of amino-PEG-alkyne (-≡) and amino-PEG-COOH (COO^-) and the azide-tagged QDs functionnalized with 4-azido-benzyl-phosphoric acid ($-N_3$). In this case, only one triazole per bounding is formed. (Lower panel) Non-selective click where the azide-alkyne CuAAC click reaction occurs at both alkyne (-≡) extremities of the bridging 1,4-Diethynilbenzene (DEB) with the azide-terminated APA ligands ($-N_3$) of the AuNPs and the azide-terminated 4-azido-benzyl-phosphoric acid ligands ($-N_3$) of the QDs. As a result, AuNPs and QDs may connect with each others via the formation of two triazole groups separated by a benzene ring.

sure that the observed aggregation process is effectively due to a CuAAC reaction and not to colloidal instabilities due to the chemical environment.

Experimental Methods

Field Emission Scanning Electronic Microscope. FESEM images were recorded using a Zeiss ultra+ scanning electron microscope, using a 3kV voltage and a working distance of 3 mm. The observations were done on 20 μL of the colloidal suspensions dried on a doped silicon wafer. Prior to the deposition, the suspensions were careful washed using Vivaspin 2 (100 kDa MWCO) concentrators to minimize the presence of salts or impurity (buffer, ascorbate, sulfate..) by three successive centrifugations at 3000 rpm during 3 min and re-dispersed in pure water. Finally, the final washed solution was diluted by a factor of 100 to reduce the issues of spontaneous aggregation of the particles during the drying process.

UV-Visible Optical Spectroscopy and Fluorescence Spectroscopy. The UV-Vis extinction spectra and the fluorescence spectra were measured using a SAFAS Xenius XC Cuvette spectrofluorometer equipped with a xenon UV lamp. Measurements were carried out in a 3 mL quartz cuvette, from 300 nm to 800 nm with a 2 nm step for the UV-Vis extinction. Fluorescence intensities were recorded from 595 nm to 680 nm, using an excitation wavelength at 585 nm.

Standard Dynamic Light Scattering. Standard DLS measurements were carried out on a commercial Cordouan Nanokin instrument operating with a red laser at 635 nm and a scattering angle of 170°. Data fitting was performed with a cumulant approach[62] and considering spherical nanoparticles.

Confocal DLS and FCS optical set-up. The confocal DLS and FCS experiments were carried out on a home-made optical setup shown in Fig.2 . The colloidal suspensions are illuminated with a tightly focused CW laser beam at $\lambda = 532$ nm, using a $\times 60$ water immersion objective with a $NA = 1.2$. The light emitted by the NPs is detected in a backscattering configuration by the objective used for the illumination. A 50 μm-diameter pinhole, placed

in the image plane of the focused beam and formed by a $f = 150$ mm lens tube, ensures the spatial filtering of the laser and reduces the sampling volume. After filtering, a $f = 30$ mm lens focuses the signal at the entrance of the monochromator. For DLS measurements, the monochromator selects the signal at $\lambda = 532$ nm whereas for FCS measurements it selects the signal at $\lambda = 615$ nm. This corresponds to the maximum of intensity of the fluorescence signal of the QDs (Figs.6b and 3b). In both cases, the light is focused by a lens doublet on a 180 μm-avalanche photodiode (APD). Each photon detected by the APD creates a TTL signal and the successive TTL are measured by the correlator, a National Instrument 6602 card, with sampling times ranging for 1 μs to 1ms, to access the rapid temporal fluctuations of the intensities.

Typical measurements consist in acquiring the scattered (resp. fluorescence) intensities during 5 to 10 s and to calculate their normalized ACF. Each measurement is repeated 5-10 times. As the fitting of the ACFs and the calculation of the hydrodynamic diameters of the particles depend on the size of the confocal volume, the latter was characterized by calibration measurements[63] that gave r_0=220 $\pm$ 20 nm, z_0=3.8 $\pm$ 0.5 μm and $w\sim$17. Uncertainties in the size of the confocal volume lead to errors of $\sim$ 20% in particle size determination. In contrast, errors due to the spreading of the diffusion vector are minimized in our geometry and do not exceed 2%.[51]

Hybrid systems obtained by selective CuAAC click reaction

Characterization by Standard Approaches

As a first-line characterization, standard FESEM, UV-Visible extinction and standard DLS experiments were performed on the colloidal solutions of the primary AuNPs and on the reference and the clicked samples. FESEM images of the citrate-capped AuNPs provided

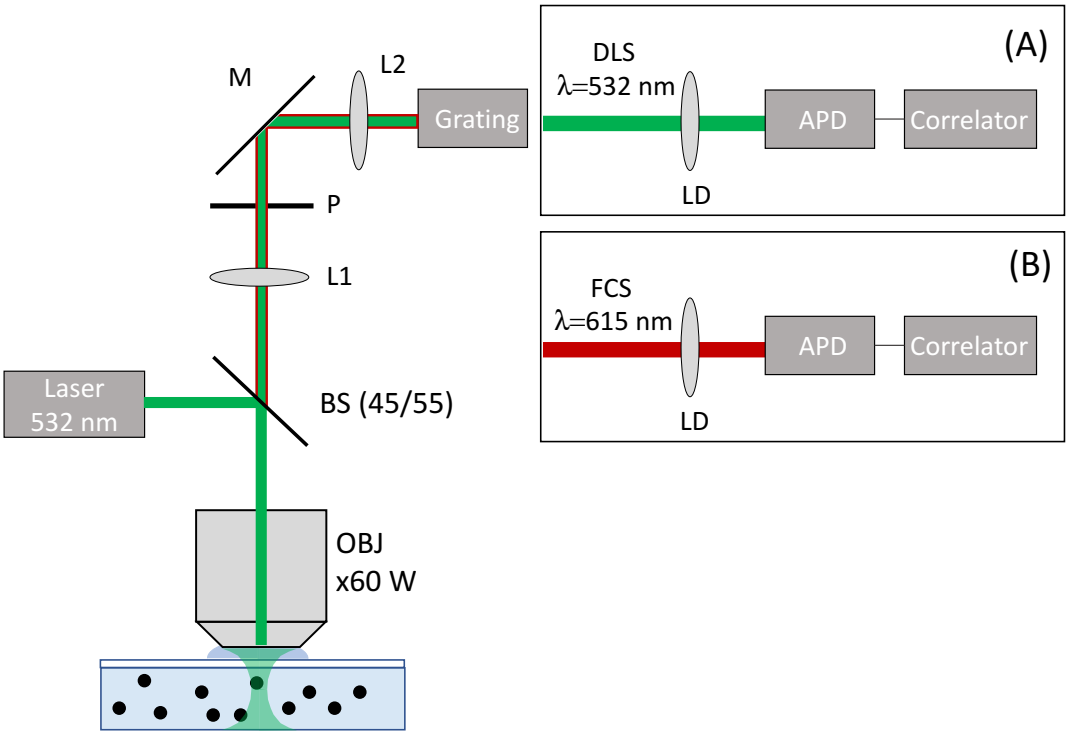

Figure 2: Schematic representation of the confocal DLS and FCS optical setup. Red and green lines represent the fluorescence signal and the Rayleigh scattering respectively. DLS (resp. FCS) measurements are done in the configuration (A) (resp. (B)). BS: beamsplitter, L: lens, LD: lens doublet, P: pinhole and M: mirror

the confirmation of the synthesis of isolated spherical AuNPs with a mean hydrodynamic diameter $d_H = 18$ nm obtained from standard DLS (Fig. S1). In parallel, their extinction spectrum, shown in Fig.3, presents the electrostatic plasmon resonance band at $\lambda = 521$ nm which is expected for AuNPs of a few tens of nanometers in diameter.[64] After functionnalization of the AuNPs with the PEG-amine/PEG-acid ligands, the extinction spectrum stays unchanged, indicating a very stable colloidal solution without any spontaneous formation of aggregates (Fig.3a). This observation was further supported by the FESEM images showing isolated AuNPs and by standard DLS which revealed an increase of the hydrodynamic diameter of the AuNPs to $d_H = 27$ nm, consistent with the grafting of long polymers to their surface (Fig. S1). The reference sample also presented a colloidal stability evidenced by a stable extinction spectrum, thereby confirming the expected absence of the click reaction. In parallel, the fluorescence spectrum shows no evidence of quenching one day after the synthesis of the sample (Fig.3b). In contrast, a noticeable aggregation process was observed for the clicked sample, as evidenced by a significant decrease in the extinction band of the isolated particles and by the presence of a second red-shifted and broad band[26] (Fig.3a). The latter is accompanied by a strong fluorescence quenching, also after 24 h of reaction. Finally, aggregates composed of both types of particles were identified by FESEM on the clicked sample (Fig.3c) while isolated or aggregates of QDs seem separated from isolated or aggregated AuNPs in the reference sample (Fig.3d).

All together, these results suggest a successful click reaction. However, they do not provide direct evidence of the involvement of the QDs in the reaction, nor details about the resulting aggregates.

Confocal DLS and FCS

To have a better understanding of the objects formed during the click reaction, confocal DLS and FCS experiments were performed. As already mentioned, confocal DLS experiments indeed probe the hydrodynamic motion of the AuNPs that scatter most of the elastic light

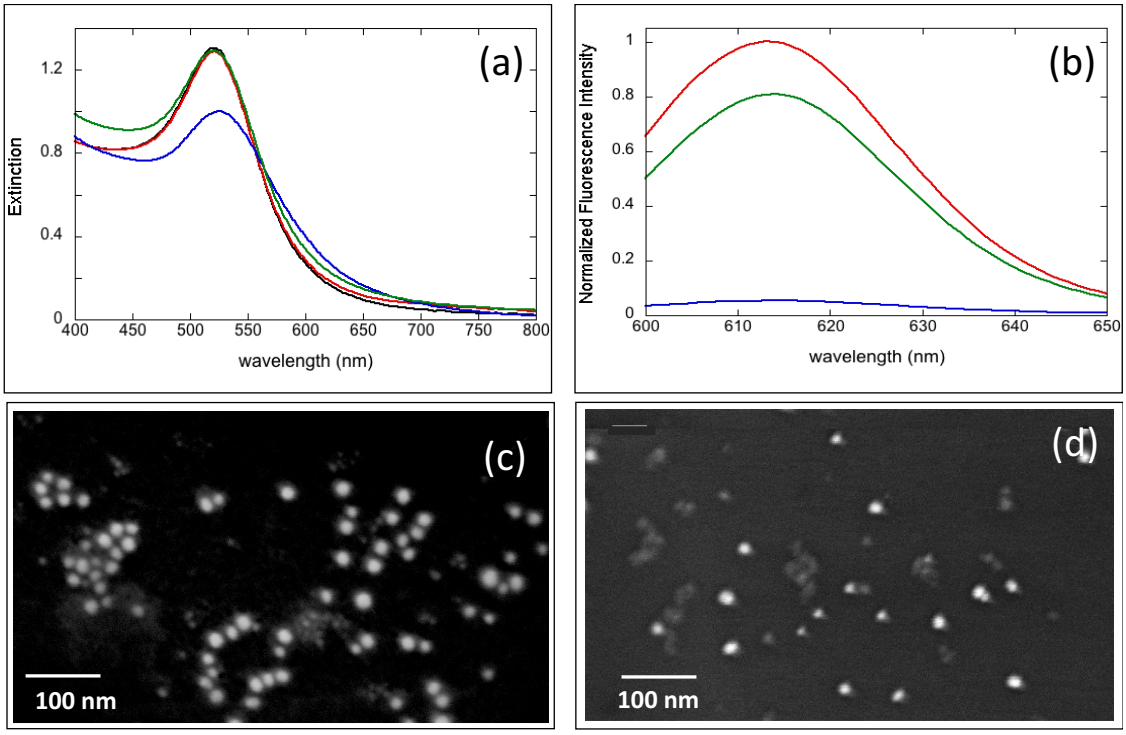

Figure 3: (a) UV-Visible extinction spectra of the citrate-capped AuNPs (black line), of the alkyne-functionnalized AuNPs (red line), and of the clicked (blue line) and reference (green line) samples after one day of reaction. (b) Fluorescence spectra of the clicked (blue) and reference (green line) samples after one day of reaction and under an excitation wavelength λ=532 nm. The spectra are normalized by the initial spectrum (red line) at the reaction time t=0 s corresponding to the addition of copper. (c) FESEM image of the clicked and (d) reference samples after one day of reaction. The brighter spheres correspond to the AuNPs while the duller and smaller objects are attributed to the QDs which have a smaller nominal size and a lower electronic conductivity.

while FCS experiments probe the hydrodynamic behavior of the QD which provide all the fluorescence signal. AuNP-QD hybrid systems will therefore have the same diffusion times in DLS and in FCS whereas isolated (or aggregates of) AuNPs or isolated (or aggregates of) QDs will present different DLS and FCS diffusion times. The values of the hydrodynamic diameters determined on the different samples are synthesized in Table 1.

Characterization of the starting QDs by FCS

To begin with, FCS experiments were performed on the azide-functionnalized QDs to determine their initial hydrodynamic diameter (that of the AuNPs being known from standard DLS). Details on the experimental methodology is given here and will stay valid for all the studies presented subsequently, including confocal DLS. In practice, the temporal fluctuations of the measured intensities, are recorded during 0.5 to 5 s, each acquisition being repeated 10 times. For each acquisition, a so-called individual ACF is derived and, at the end of the acquisition, a mean ACF averaged over all the repetitions is also calculated to reduce the noise. In FCS, the data analysis consists in fitting the experimental ACFs accordingly to Eq. 2, to determine the value of the characteristic time τ_D from which D and the corresponding hydrodynamic diameter d_H are calculated (see Theoretical Background section). The experiments were conducted at a room temperature $T = 22°\text{C}$ for which $\eta(22°C) = 0.95$ mPa.s and therefore $d_H/\tau_D = 37 \pm 7$ nm/ms.

The mean experimental FCS ACF is shown in Fig. 4, along with the individual ones composing the mean value. The latter are very similar to each other, indicating that the QDs solution is homogeneous. The mean ACF was fitted with a characteristic time $\tau_D = 0.4$ ms corresponding to a mean diameter $d_H = 14.8 \pm 2.5$nm for the QDs (Table 1), a value slightly higher than the nominal physical diameter due to the presence of the clickable ligands. The fitting of the individual FCS ACFs leads to different characteristic times ranging from 0.3 ms to 0.5 ms i.e to a size distribution ranging from 11 to 19 nm and no large aggregates were observed.

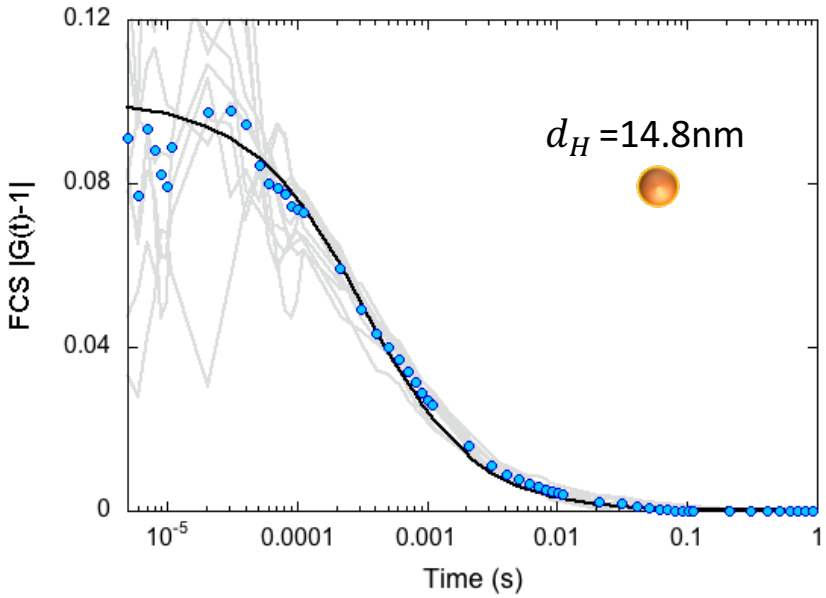

Figure 4: Mean experimental FCS ACF (dots) obtained by averaging ten individual ACFs (gray lines) measured on azide-functionnalized QDs. The best fit of the mean ACF (black line) was obtained for τ_D=0.4 ms corresponding to a mean diameter d_H=14.8 nm.

Identification of the formed hybrid systems.

Confocal DLS and FCS measurements were then done on the reference and the clicked samples. In DLS, the data analysis consists in fitting the experimental ACFs accordingly to Eq. 1, to determine the values of the characteristic times τ_c and τ_D. The determination of the hydrodynamic diameter d_H from τ_D is the same in DLS as in FCS, whereas that from τ_c depends on the scattering vector q which is determined by the experimental configuration ($\theta = 180°$ and $\lambda = 532$ nm) and the nature of the solvent (water, $n = 1.33$). Here DLS experiments were also conducted at a room temperature $T = 22°$C such that τ_D=37.5±7 nm/ms and τ_c=449±10 nm/ms.

The clicking process being selective, we expect that a successful CuAAC reaction ideally results in the formation of a colloidal solution of hybrid AuNP-QD aggregates which are

detected similarly in DLS and FCS. However, it is possible to encounter an intermediate scenario where hybrid systems coexist with unreacted primary particles. This occurrence depends on various factors, including the efficiency of the CuAAC reaction and the relative concentrations of reactants. In such situations, disparities in the DLS and FCS ACFs are observed thus giving access to the differentiation between these two regimes. In the present case, both regimes coud be identified in the clicked sample as the CuAAC reaction was sufficiently optimized to yield a final colloidal solution of hybrid systems, yet slow enough to permit the observation of the partial clicking regime at the beginning of the reaction. Additionally, the absence of binding between the AuNPs and the QDs in the reference sample was confirmed. These different results are illustrated in Fig.5 that presents the mean DLS and FCS ACFs obtained on both samples.

In the case of the reference sample, the mean experimental DLS ACF (Fig.5a) is fitted with τ_D=0.74 ms and τ_c=0.06 ms, giving a hydrodynamic diameter d_H=27±5 nm for the AuNPs, in perfect agreement with the size of the alkyne-functionnalized AuNP determined by standard DLS value (Table 1). In parallel, the mean FCS ACF presents a characteristic time τ_D=0.45 ms giving d_H=16.8±3 nm also in agreement with isolated QDs. The AuNPs and the QDs are thus mixed together in the same solution, each maintaining its original colloidal state.

The first experiments on the clicked sample were carried out during the few hours following the addition of the copper. The partial clicking stage was identified by comparing the mean DLS and FCS ACFs which differed and yet presented larger diffusion times than those in the reference sample (Fig.5b). In DLS, the diffusion times obtained are τ_D=0.95 ms and τ_c= 0.077 ms giving d_H=35±6 nm (Table 1). With d_0=27 nm for the primary AuNPs and d_1=14.8 nm for the primary QDs, and using the hydrodynamic bead model,[53,54] we find that this value fits in with the formation of small aggregates, which is consistent with a reaction that begins. Indeed, for AuNP-QD dimers, $\alpha(2)$=0.907 and d_A=31 nm and for QD-AuNP-QD trimers, $\alpha(3)$=0.83 and d_A=36 nm (see Theoretical Background Section). Additionally,

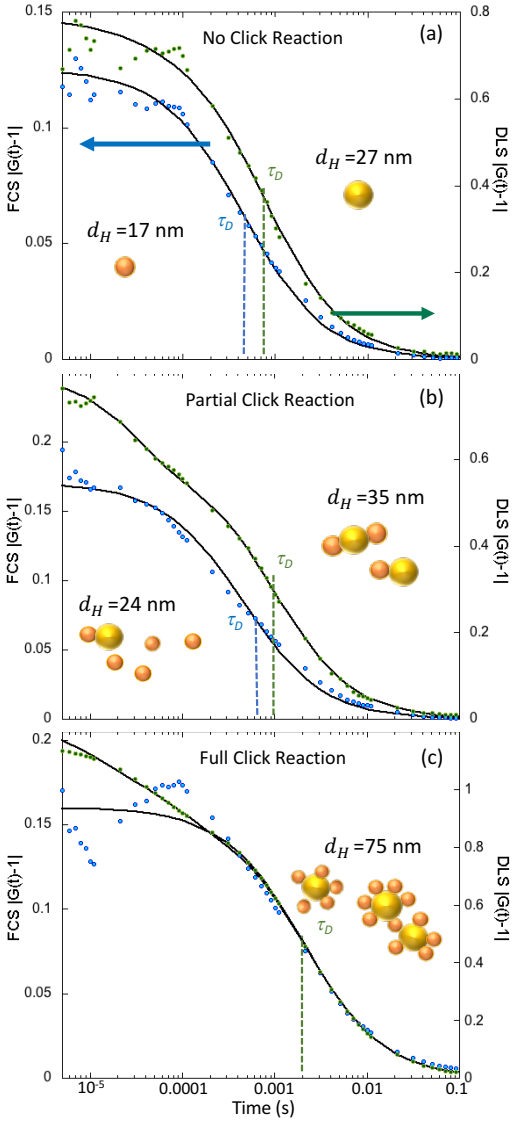

Figure 5: Experimental (dots) and calculated (lines) ACFs obtained in FCS (blue) and in DLS (green) on the reference sample (a) and on the clicked sample at the initial stage of clicking (b) and when the reaction is finished (c). In (a) the DLS diffusion time corresponds to the motion of the primary AuNP and the FCS diffusion times to that of the primary QDs. At the beginning of the reaction (b), small aggregates of dimers and trimers form while most of the QDs are still free. Finally, when the reaction is finished (c) the colloidal solution contains hybrid systems containing in average 10-12 particles, identically identified by DLS and by FCS.

the individual ACFs present a spreading of the τ_D values ranging from 0.8 to 1.4 ms (i.e d_H=30 to 52 nm) which indicates that the solution is rather heterogeneous and that larger aggregates are also formed. The accurate description of the larger aggregates is difficult to do as the number of AuNPs (n), contained in a hybrid system of n_s particles, is not accessible. Yet, we can define an upper (resp. lower) limit of the number n_s, by considering that the aggregates are purely composed of QDs (resp. AuNPs). Using the values of $\sqrt[3]{n_s}\alpha(n_s)$ given in Ref.[53] and reproduced in the SI4, we find that d_H=52 nm could correspond to a 8-QDs aggregate or to a 4-AuNPs aggregate. As the initial molar concentration of AuNPs:QDs is 1:25, one can reasonably expect that the aggregates are composed of more QDs than AuNPs such that n_s= 6-7 and n=1-2 seem reasonable values. In this case, $\alpha \sim 0.7$[53] and $d_{eq} = d_0 \sqrt[3]{n + (n_s - n)(d_1/d_0)^3}$, which leads to hybrid systems of diameters of $d_A \sim 54 \pm 5$ nm.

In parallel to these DLS results, the mean FCS ACF exhibits a diffusion time τ_D=0.65 ms which corresponds to a diameter d_H=24±4 nm for the objects containing QDs, while the individual ACFs are clearly of two kinds: those exhibiting characteristic times ranging from 0.4 to 0.55 ms with a mean value τ_D= 0.45 ms, representative of the isolated QDs, and those with larger characteristic times ranging from 0.6 to 1.1 ms, with a mean value τ_D= 0.9 ms, signing the presence of the larger objects observed in DLS. This result indicates that most of the QDs in solution are still free, which is in accordance with the DLS results suggesting that the formed aggregates only contain a small fraction of the total number of QDs.

After one day, the clicking reaction is finished and the mean DLS and FCS ACFs exhibit the same diffusion time τ_D=2 ms, bigger than previously (Fig.5c). The equality of the diffusion times of both ACFs indicates that the measured dynamic properties of the systems are dominated by those of the hybrid systems, whose mean size is d_H=75±15 nm. In parallel, the individual ACFs give τ_D values spreading from 1 to 3.5 ms (i.e d_H=38 to 110 nm) that confirm the size heterogeneity of the formed objects. As before, according to ref.,[53] the mean diameter value could correspond a chain of n_S=14 QDs or to n_s=6 AuNPs. Within

this range, intermediate value of n_s=10-12 can be considered. At such values of n_s, the coefficient α varies slowly and is ∼0.58. Considering d_A=70-80 nm as acceptable values, we find that n=1-3 AuNPs. The number of QDs per AuNP is thus smaller than the initial 25:1 QDs:AuNP ratio. This suggests that non connected QDs are still in solution. However, their presence is not detected by the FCS measurement, despite the quenching of the connected QDs. This is due to the fact that, in correlation spectroscopy, the amplitude and frequency of the temporal fluctuations are more relevant than the absolute value of the intensity of the signal. Hence the large and diluted hybrid systems generate important fluctuations in the measured fluorescence that overshadow those caused by smaller and more concentrated QDs. Finally, we point out that some ACFs exhibit additional time-decays at short characteristic times (5-50 μs). Such an effect is usually attributed to the rotation, within the observation volume, of anisotropic shaped particles and can also be quantified through hydrodynamic models[54,56] . However, such analyses could not be conducted in the present paper due to the possible blinking of the QDs that may also create time-decays within this time range.[65]

Table 1: Summary of the measured hydrodynamic diameters for the selective click reaction

Sample	d_H from DLS (nm)	d_H from FCS (nm)
Citrate-capped AuNP	18	-
Azide-capped AuNP	27	-
Azide-capped QD	-	14.8
Partially Clicked sample	35	24
Completely Clicked sample	75	75
Reference sample	27	17

Hybrid systems obtained by non-selective CuAAC click reaction

Characterization by Standard Approaches

As for the selective click case, the samples were first characterized by standard FESEM, UV-Visible extinction and DLS experiments. This approach confirms the formation of spherical citrate-capped AuNPs, with a size distribution centered at d_H = 28 nm (Fig. S2) and an electrostatic plasmon resonance centered at λ=528 nm (Fig.6a). After the functionalization step with APA ligands, the colloidal stability of the AuNPs is largely maintained: FESEM images show isolated AuNPs (Fig. S2) and the plasmonic resonance is not shifted (Fig.6a). However, the latter slightly decreases in intensity when a weak band appears around λ = 650 nm thus indicating the formation of a limited number of aggregates.[26] As a result, the mean diameter measured by DLS, that averages all the particles, increases to d_H = 36 nm (Fig. S2), a value that cannot be solely attributed to the ligands which are short and do not exceed 3-4 nm.

The extinction spectrum of the clicked sample (Fig.6a) shows a marked decrease in the electrostatic band and an increase and red-shift of the second broader band, signifying the presence of larger and more numerous aggregates. However, it is not possible to determine the contribution of the QDs to these aggregates, the extinction coefficient of the QDs being several orders of magnitude smaller than that of the AuNPs. Moreover, the reference sample exhibits the same behavior (Fig.6a). In parallel, a 50 % quenching of the initial fluorescence intensity was observed after one day, but also on both samples (Fig.6b). At this point, the observed colloidal instability and the decrease of fluorescence are thus more likely due to the reagents (EtOH, DEB and/or Cu) than from the clicking process itself. The FESEM images did not shed much more light on the clicking process. Indeed, small AuNP-QD system were seldom identified in the clicked sample but the same type of object also appeared on the reference sample (Fig.6d).

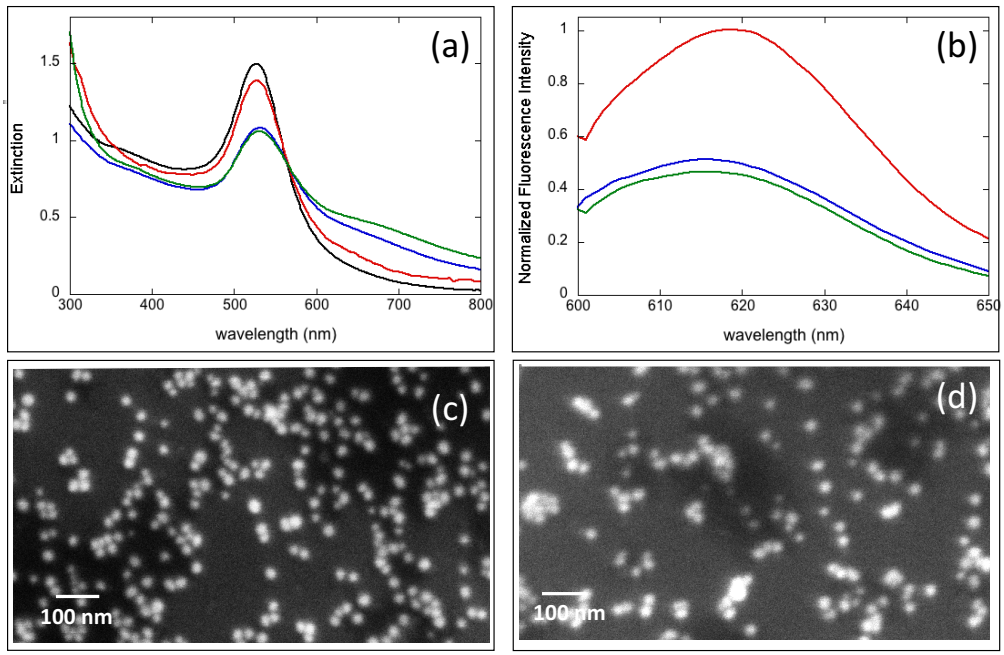

Figure 6: (a) UV-Visible extinction spectra of the citrate-capped AuNPs (black line), of the APA-functionnalized AuNPs (red line), and of the clicked (blue line) and reference (green red) samples after one day of reaction. (b) Fluorescence spectra of the clicked (blue line) and reference (green line) samples after one day of reaction and under an excitation wavelength $\lambda = 532$ nm. The spectra are normalized by the initial spectrum (red line) at the reaction time t=0 s corresponding to addition of copper. (c) FESEM image of the clicked and (d) reference samples after one day of reaction. The brighter spheres correspond to the AuNPs while the duller and smaller objects are attributed to the QDs which have a smaller nominal size and a lower electronic conductivity.

If it is quite clear that AuNPs have partially aggregated, the role of the QDs and the effectiveness of the click reaction itself stay unrevealed by these experimental approaches. To obtain more information, SERS (Surface Enhanced Raman Scattering) were carried out. The SERS spectra measured on the clicked and reference samples are presented in Fig. 7. Both show the Raman band of the ethanol solvent while only the spectrum of the clicked sample shows the SERS signal of the triazole and benzene ring[66] (1177 cm^{-1} and 1533 cm^{-1} for the triazole and 1153 cm^{-1} and 1606 cm^{-1} for the benzene). This gives a clear and unambiguous signature of CuAAC induced AuNP-AuNP binding in the clicked sample which does not occur in the reference sample. However, and as previously, the possible connection between the QDs and the AuNPs cannot be probed by SERS as this effect is due to the electromagnetic resonances of AuNPs aggregates and occurs for molecules located between AuNPs but not within QD-AuNP interstices.

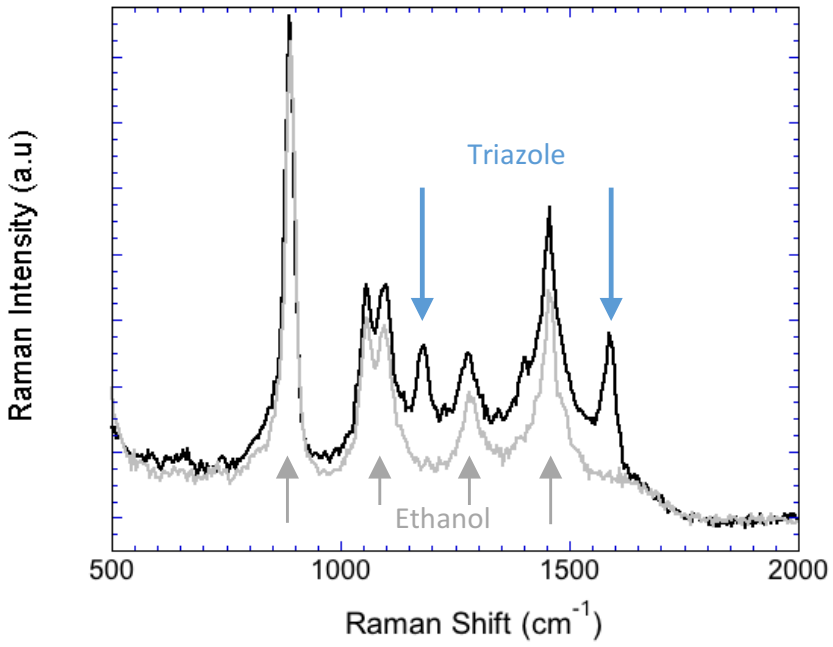

Figure 7: Raman spectra of the clicked sample (black line) and of the reference sample (gray line) . The reference sample only exhibits the expected ethanol Raman bands whereas two supplementary bands signing the presence of triazole and benzene[66] are observed in the clicked sample at 1177 cm^{-1} and at 1590 cm^{-1}.

Confocal DLS and FCS results

As previously, confocal DLS and FCS experiments were performed to gain a better understanding of the samples. However, the current case is more complicated due to the presence of AuNPs aggregates and to the possibility of a click reaction between both types of NPs. Moreover, the standard approaches failed to ascertain the success of the reaction, and to determine the diameter of the isolated APA-functionalized AuNPs.

Characterization of the starting APA-functionalized AuNPs To begin with, confocal DLS experiments were thus performed on the APA-functionnalized AuNPs (the QDs being the same as for the selective click reaction). The experiments were conducted at a room temperature $T = 28°$C with $\eta(28°C) = 0.83$ mPa.s, such that $d_H/\tau_D = 44 \pm 8$ nm/ms and $d_H/\tau_c = 500 \pm 10$ nm/ms. The values of the hydrodynamic diameters determined on the different samples hereafter are synthesized in Table 2.

Figure 8 shows the mean experimental DLS ACF of the APA-functionnalized AuNPs, averaged over ten different acquisitions. Its fitting was done with τ_c=0.07 ms and $\tau_D = 0.95$ ms giving an average hydrodynamic diameter d_H=38±10 nm, in good agreement with standard DLS results (Fig. S2). It is expected that the mean ACF gives results consistent with approaches probing large volumes (such as standard DLS and UV-Visible spectroscopy) as the assumption of ergodicity, conventionally made for colloidal suspension, allows to consider that the averaging of different data measured in a small volume (time averaging) is analogous to a spatial averaging obtained by probing a bigger volume. A benefit of confocal DLS is that only a very small volume of the sample is probed, typically $V_c \sim 1f$L. With AuNPs colloids at 6 nM, the mean local concentration is ∼3.6 AuNP/V_c (while the instantaneous local concentration obeys a Poisson law distribution), such that the objects crossing the confocal volume are almost individually observed. Therefore, the different scattering events no longer occur simultaneously as in standard DLS, but occur one after the other. A large aggregate, with a high scattering cross section, will create isolated and easily identifiable bursts in the recorded intensities that will significantly modify the resulting ACF. At sufficiently low con-

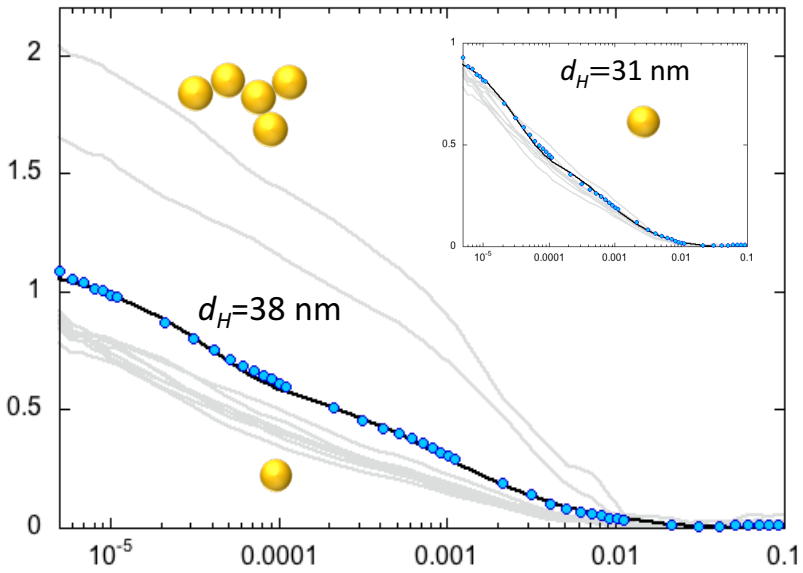

Figure 8: Mean experimental DLS ACF (dots) obtained by averaging ten individual ACFs (gray lines) measured on APA-functionnalized AuNPs. The best fit of the mean ACF (black line) was obtained for τ_D=0.95 ms corresponding to a mean diameter d_H=38 nm. Most of the individual ACFs are similar, and their averaged ACF is fitted with τ_D=0.74 ms corresponding to a mean diameter d_H=31 nm (inset). They account for the the motion of isolated AuNPs. The second kind of individual ACF is significantly modified due to the presence of at least one aggregate in V_c during the acquisition time.

centration of such aggregates, these ACFs can be treated independently (or isolated) from those of the smaller scatterers of interest. As an example, the individual ACFs obtained on the APA-functionnalized AuNPs are also shown in Fig. 8. They present two very distinct kinds of ACFs: when an aggregate is detected, the ACF has an increased $\frac{c^2}{\langle N \rangle}$ value, as the signal to noise increases, and large characteristic times (here τ_D=1.6 ms) corresponding to hydrodynamic diameter much larger than the mean hydrodynamic diameter. In contrast, in most ACFs, no aggregates are detected and the ACFs give access to the dynamic properties of the other particles in solution. In the present case, the individual ACFs free of aggregates were quite similar and exhibited characteristic times τ_D ranging from 0.4 ms to 1 ms, corresponding to hydrodynamic diameters between 17 nm and 43 nm. Moreover, their averaged ACF is fitted with $\tau_D = 0.74$ ms and $\tau_c = 0.058$ ms which gives a diameter $d_H = 31 \pm 8$ nm for the staring particles (Table 2). Both the size dispersion and the mean diameter are in perfect agreement with the size distribution of the citrate-capped AuNPs (Fig. S2) slightly increased by the presence of the APA ligands.

Table 2: Summary of the measured hydrodynamic diameters in the non-selective click process.

Sample	d_H from DLS (nm)	d_H from FCS (nm)
Citrate-capped AuNP	28	-
Azide-capped AuNP	31	-
Azide-capped QD	-	14.8
Click sample	39	27
Reference sample	31	12

Identification of the formed hybrid systems. Similar experiments were carried out on the reference and clicked samples. In both samples, the extinction spectra revealed the formation of large AuNP aggregates presumably more likely due to a slight colloidal instability than to the click reaction. This assumption was first confirmed by the intensities recorded in

confocal DLS then in FCS. The Rayleigh intensities may indeed present very intense bursts which never appear in the fluorescence intensities, thus confirming that the QDs and the click reaction are not significantly involved in the existence of these large aggregates. An

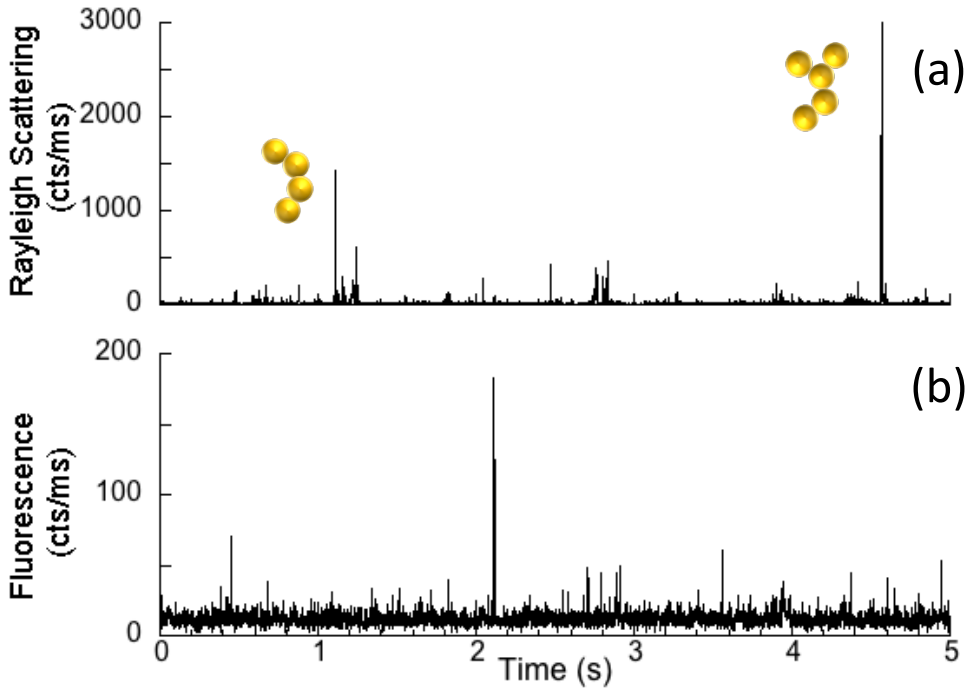

Figure 9: Rayleigh (a) and fluorescence (b) intensities integrated over 1 ms and measured on the clicked sample. AuNPs aggregates are schemed by the yellow spheres and appear in DLS as strong intensity burst. Such events are not observed in FCS.

example is given in Figure 9 for the clicked sample, the same behavior being observed on the reference sample. The access to the colloidal state of the smaller particles in solution (isolated AuNPs or QDs and formed hybrid systems) was thus realized by analyzing the ACFs obtained from intensities free of such bursts.

The resulting mean confocal DLS and FCS ACFs measured on the clicked sample are shown in Fig.10a and 10b respectively. Let us recall that the solvent is a water:ethanol mixture at 50:50 in volume whose viscosity is significantly higher than that of water or ethanol alone.[67] In the present case, its value was determined by performing confocal DLS experiments on size-calibrated polystyrene beads in such a mixture (Fig.S3) and was found to be 2.7±0.1 times larger than that of water, in good agreement with Ref.[67] The relationships be-

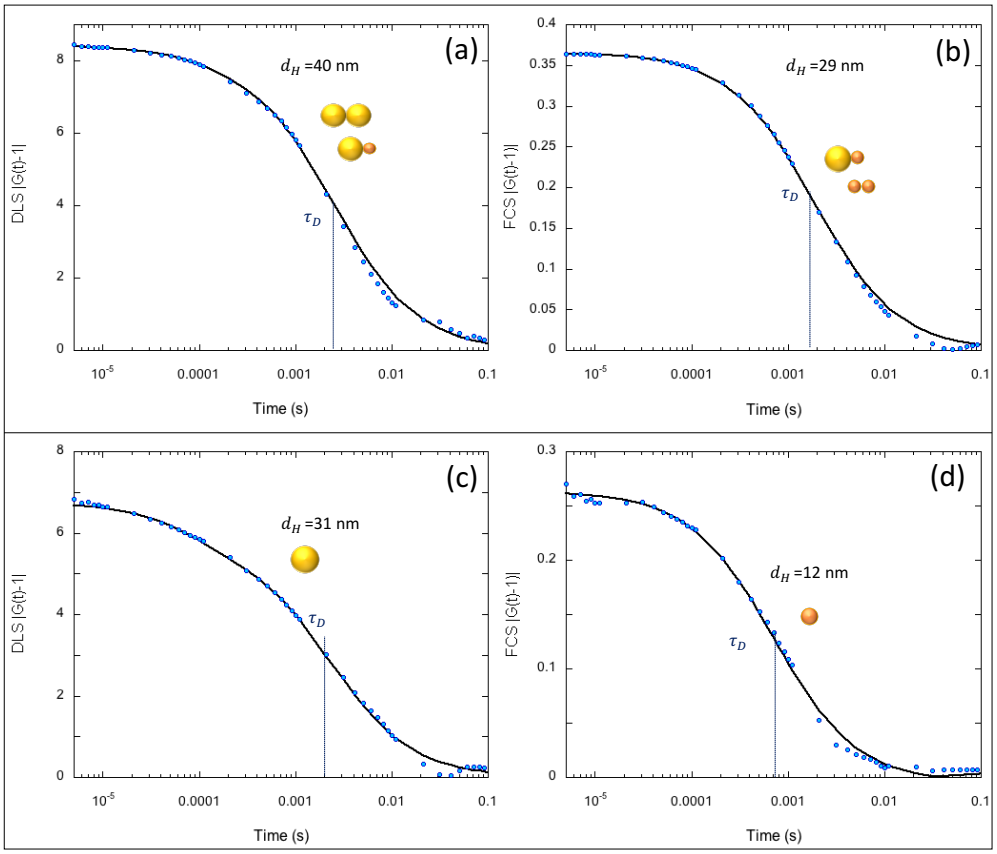

Figure 10: Mean experimental (dots) and calculated (lines) confocal DLS ACFs (a) and FCS ACFs(b) of the clicked sample. In both cases the click reaction is detected via the increase of the diffusion time τ_D with respect to that of the primary AuNPs and QDs. The as-formed and probed aggregates are represented by yellow spheres for AuNPs and orange spheres for QDs. In contrast, no click reaction occurred in the reference sample where the diffusion time is that of the isolated primary AuNPs in DLS (c) and of the QDs in FCS (d).

tween hydrodynamic diameters and characteristic times therefore become $\tau_D = 16.3$ nm/ms and $d_H/\tau_c = 194$ nm/ms with $n = 1.36$ and $T = 28°$C.

The DLS ACF was fitted with $\tau_D = 2.5$ ms and $\tau_c = 0.2$ ms giving $d_H = 40 \pm 7$ nm and the FCS ACF was fitted with $\tau_D = 1.8$ ms giving $d_H = 29 \pm 5$ nm (Table 2). In both cases, the diameters are larger than those of the primary AuNPs and QDs, which is in favor of a successful linking between them. This assumption is supported by the fact that the size increase is lower in DLS than in FCS. The QDs are indeed much smaller than the AuNPs and the formation of AuNP-QD bond does not significantly modify the motion of the AuNPs but more significantly that of the QDs. Finally, such a change in diameters is not observed in the reference sample whose DLS and FCS ACFs are presented in Fig. 10c and 10d respectively. The latter indeed exhibits diffusion times $\tau_D = 2$ms in DLS and $\tau_D = 0.75$ ms in FCS corresponding to $d_H = 32 \pm 6$nm for the AuNPs and $d_H = 12 \pm 2$ nm for the QDs (Table 2). Both values correspond to that of the primary particles, the diameter of the QDs being here sightly smaller than in Fig. 8 due to the absence of clickable ligands for the QDs in the reference sample.

The determination of the nature of the objects formed during the chemical click reaction is supported by the hydrodynamic bead model[53,54] (see Theoretical Background Section). In the most simple case of dimers, we have $\alpha(2)$=0.907. Thus, considering our primary AuNPs, with $d_0 = 31$ nm, and the primary QDs, with $d_1 = 14.8$ nm, the hydrodynamic diameter of a AuNP-AuNP dimer is $d_A = 43$ nm and that of a AuNP-QD dimers is $d_A = 35$ nm. Interestingly we see that the DLS measurements revealed a hydrodynamic diameter of intermediate value $d_H = 40$ nm which fits with an averaged contribution of AuNP-AuNP dimers and that of AuNP-QD dimers. In parallel, FCS measurement gave a value $d_H = 29$ nm which also fits in with an averaged contribution of the AuNP-QD dimers ($d_A = 35$ nm) and that of the QD-QD dimers ($d_A = 20$ nm). Now, if trimers formed by identical spheres are considered, α=0.83 such that $d_A = 54$ nm for AuNP trimers, $d_A = 26$ nm for QD trimers and $d_A = 40$ nm for AuNP-QD-QD trimers. The formation of AuNPs trimers is deemed

unlikely as the value of d_A is high compared to the DLS results. However, the formation of QDs and AuNP-QD-QD trimers cannot be excluded.

In conclusion of these analyses, we can affirm that the non-selective click reaction was successfully controlled and that it led to the formation of small aggregates of the different particles, essentially dimers or trimers. The clicked and reference samples also contain large AuNP scatterers due to the reaction reactants. Their concentration is, however, very low as can be estimated looking back at the recorded intensities presented in Fig.9a. Knowing that the transit time through the confocal volume is $\sim$ 2 ms and that there are initially $\sim$ 0.6 AuNP/V_c, it can be roughly estimated $\sim$1500 AuNPs are probed during the 5s of measurements when only 2 to 3 bursts are detected during the same duration. The ratio of aggregates/AuNP is thus around 2 ‰.

Conclusion

Hybrid systems consisting of colloidal CdSe-ZnS QDs connected to AuNPs were synthesized by CuAAC click reactions. Two different reactions were developed: a selective reaction where only AuNP-QD bonds can form and a non-selective reaction where bonding can occur between any type of particles. Combined confocal DLS and FCS experiments were conducted to probe the hydrodynamic motion of the AuNPs (by DLS) and that of the QDs (by FCS), merging them to determine the nature of the hybrid systems. In parallel, electron microscopy and static optical spectroscopy measurements were also performed. These standard means qualitatively highlighted the success of the selective click reaction but they provided limited information on the nature of the hybrid systems. DLS and FCS enabled the tracing of the reaction evolution: from the non-connected case, where AuNPs and QDs present different motions, to the initial state of the clicking process, where AuNP-QD dimers and trimers are formed while most of the QDs remain free in solution and finally to the final state of the

reaction where large and size-heterogenous AuNP-QD aggregates have formed. Their mean size corresponds to aggregates containing 10-12 particles and with a ratio of 4-5 QDs per AuNPs. In the case of the non-selective click reaction, the success of the click reaction could not be ascertained by electron microscopy and static optical spectroscopy measurements. However, this issue was addressed by DLS and FCS, and we demonstrated that the synthesized hybrid systems are essentially composed of AuNP-QD dimers and trimers. We believe that combining confocal DLS and FCS and obtaining such quantitative information is highly relevant for a deeper understanding of the physicochemical properties of hybrid systems.

Acknowledgement

This work was supported by the Agence Nationale de la Recherche (ANR) through the ANR-18-CE93-0004 project and the Swiss National Science Foundation (project 200021L-182078).

Supporting Information Available

- SI-1: SEM image and size distribution of the initial and Alkyne functionalized gold nanoparticles
- SI-2: SEM image and size distribution of the initial and azide functionalized gold nanoparticles
- SI-3: Normalized auto-correlation functions measured by confocal DLS on polystyrene beads in an aqueous medium and in a water:ethanol 1:1 v:v mixture.
- SI-4: Graphs and values of the coefficient $\alpha(n_s)$ and of $\sqrt[3]{n_s}/\alpha(n_s)$

References

(1) Sukharev, M.; Nitzan, A. Optics of Exciton-Plasmon Nanomaterials. *J. Phys.: Condens. Matter*, **2017**, 29, 443003-4433003-7.

(2) Achermann, M. Exciton-Plasmon Interactions in Metal-Semiconductor Nanostructures. *J. Phys. Chem. Lett.*, **2010**, 1, 2837-2843.

(3) Govorov, A. O.; Bryant, G. W.; Zhang, W.; Skeini, T.; Lee, J.; Kotov, N. A.; Slocik, J. M.; Naik, R. R. Exciton-Plasmon Interaction and Hybrid Excitons in Semiconductor-Metal Nanoparticle Assemblies. *Nano. Lett.*, **2006**, 6(5), 984-994.

(4) Kosionis, S. G.; Paspalakis, E. Energy Absorption of an Exciton-Biexciton System in a Quantum Dot-Metal Nanoparticle Hybrid. *Physica B*, **2022**, 643, 414186-414194.

(5) Ge, R-C.; Van Vlack, C.; Yao, P.; Young, J. F.; Hughes, S. Accessing Quantum Nanoplasmonics in a Hybrid Quantum DotMetal Nanosystem: Mollow Triplet of a Quantum Dot Near a Metal Nanoparticle. *Phys. Rev. B*, **2013**, 87, 205425-1-8.

(6) Ridolfo, A.; Di Stefano, O.; Fina, N.; Saija, R.; Savata, S. Quantum Plasmonics with Quantum Dot-Metal Nanoparticle Molecules: Influence of the Fano Effect on Photon Statistics. *Phys. Rev. Lett.*, **2010**, 105, 263601-1-4.

(7) Bitton, O.; Gupta, S. N.; Haran, G. Quantum Dot Plasmonics: from Weak to Strong Coupling. *Nanophotonics*. **2019**, 8(4), 559-575.

(8) Singh, M. R. Enhancement of the Second-Harmonic Generation in a Quantum DotMetallic Nanoparticle Hybrid System. *Nanotechnology*, **2013**, 24,125701-125706.

(9) Liu, X.; Kongsuwan, N.; Li, X.; Zhao, D.; Wu, Z.; Hess, O.; Zhang, X. Tailoring the Third-Order Nonlinear Optical Property of a Hybrid Semiconductor Quantum dot-Metal Nanoparticles: From Saturable to Fano-Enhanced Absorption. *J. Phys. Chem. Lett.*, **2019**, 10, 7594-7602.

(10) Hou, W.; Cronin, S. B. A Review of Surface Plasmon Resonance-Enhanced Photocatalysis. *Adv. Funct. Mat.*, **2013**, 23(13), 1612-1619.

(11) Dabbous A.; Bauer P.; Marcucci C.; Périé, S.; Gahlot, S.; Lombard, C.; Caillat, S.; Ravanat, J-L.; Mouesca, J-M.; Kodjikian S.; Barbara A.; Dubois F.; Maurel, V. Hybrid CdSe/ZnS Quanum Dot-Gold Nanoparticle Composites Assembled by Click Chemistry: Towards Affordable and Efficient Redox Photocatalysts Working withVisible Light. *ACS Appl. Maer.Interfaces*, **2023**, 15, 56167-56180.

(12) Ji, B.; Giovanelli, E.; Habert, B.; Spinicelli, P.; Nasilowski, M.; Xu, X.; Lequeux, N.; Hugonin, J.-P.; Marquier, F.; Greffet, J.-J.; Dubertret, B. Non-Blinking Quantum Dot with a Plasmonic Nanoshell Resonator. *Nature Nanotech.*, **2015**, 10 (2), 170175.

(13) Yang, T.-T.; Chen, W.-T.; Hsu, Y.-J.; Wei, K.-H.; Lin, T.-Y.; Lin, T.-W. Interfacial Charge Carrier Dynamics in CoreShell Au-CdS Nanocrystals. *J. Phys. Chem. C*, **2010**, 1114 (26), 141411420.

(14) Hoang, T. B;; Akselrod, G.M.; Argyropoulos, C.; Huang, J.; Smith, D.R.; Mikkelsen, M.H. Ultrafast Spontaneous Emission Source using Plasmonic Nanoantennas. *Nat. Commun.*, **2015**, 6, 7788-77.

(15) Wang, H.; Wang, H-Y.; Toma, A.; Yano, T-A.; Chen, Q-D.; Xu, H-L.; Sun, H-B.; Zaccaria, R. P. Dynamics of Strong Coupling between CdSe Quantum Dots and Surface Plasmon Polaritons in Subwavelength Hole Array *J. Phys. Chem. Lett.*, **2016**, 7, 46484654.

(16) Gomez, D. E.; Vernon, K.C.; Mulvaney, P.; Davis, T.J. Surface Plasmon Mediated Strong Exciton-Photon Coupling in Semiconductor Nanocrystals. *Nano. Lett.*, **2009**, 10, 274278.

(17) Zhang, J.; Badugu, R.; Lakowicz, J. R. Fluorescence Quenching of CdTe Nanocrystals by Bound Gold Nanoparticles in Aqueous Solution. *Plasmonics*, **2008**, 3, 3-11.

(18) Cohen-Hoshen, E., Bryant, G. W.; Pinkas, I.; Sperling, J.; Bar-Jospeh, I. ExcitonPlasmon Interactions in Quantum DotGold Nanoparticle Structures. *Nano Lett.*, **2012**, 12, 4260-4264.

(19) Guo, Y; Deng, Z. DNA Directed Self-Assembly of Fluorescent Colloidal Semiconductor Quantum Dots and Plasmonic Metal Nanoparticles Heterogeneous Nanomaterials *Chin. J. Chem.*, **2016**, 34, 259-264.

(20) Fernandez, M.; Urvoas, A.; Even-Hernandez, P.; Burel, A.; Mériadec, C.; Artzner, F.; Bouceba, T.; Minard, P.; Dujardin, E.; Marchi, V. Hybrid gold nanoparticlequantum dot self- assembled nanostructures driven by complementary artificial proteins. *Nanoscale*, **2020**, 12, 4612-4621.

(21) Lee, P. C.; Meisel, D. Adsorption and Surface-Enhanced Raman of Dyes on Silver and Gold Sols. *J. Phys.Chem.*, **1982**, 86, 3391-3395.

(22) Turkevich, J.; Stevenson, P. C.; Hillier, J. A Study of the Nucleation and Growth Processes in the Synthesis of Colloidal Gold. *Discuss. Faraday Soc.*, **1951**, 11, 55-75.

(23) Frens, G. Controlled Nucleation for the Regulation of the Particle Size in Monodisperse Gold Suspensions. *Nat. Phys. Sci.*, **1973**, 241(105), 20-22.

(24) Talapin, D.V.; Lee, J. S.; Kovalenko, M.V.; Shevchenko, E. V. Prospects of Colloidal Nanocrystals for Electronic and Optoelectronic Applications. *Chem. Rev.*, **2010**, 110, 389-458.

(25) Alivisatos, A. P. Semiconductor Clusters, Nanocrystals, and Quantum Dots. *Science*, **1996**, 271, 933-937.

(26) Blatchford, C. G.; Campbell, J. R.; Creighton, J. A. Plasma Resonance- Enhanced Raman Scattering by Adsorbates on Gold Colloids: The Effects of Aggregation. *Surf. Sci.*, **1982**, 120, 435-455.

(27) Jain, P. K.; El-Sayed, M. A. Surface Plasmon Coupling and Its Universal Size Scaling in Metal Nanostructures of Complex Geometry: Elongated Particle Pairs and Nanosphere Trimers. *J. Chem. Phys. C*, **2008**, 112, 4954-4960.

(28) Link, S; El-Sayed, M. A. Size and Temperature Dependence of the Plasmon Absorption of Colloidal Gold Nanoparticles. *J. Chem. Phys. B*, **1999**, 103, 8410-8426.

(29) Artuso, R. D.; Bryant, G. W. Optical Response of Strongly Coupled Quantum Dot-Metal Nanoparticle Systems: Double Peaked Fano Structure and Bistability. *Nano Lett.*, **2008**, 8, 2106-2011.

(30) Artuso, R. D.; Bryant, G. W.; Garcia-Etxarri, A.; Aizpurua, J. Using local fields to tailor hybrid quantum-dot/metal nanoparticle systems. *Phys. Rev. B*, **2011**, 83, 235406-1-9.

(31) Gueroui Z., Libchaber A. Single-Molecule Measurements of Gold-Quenched Quantum Dots. *Phys. Rev. Lett.*, **2004**, 93(16), 166108-1-4.

(32) Jin, L-H.; Kwon, B-J.; Cho, Y-H. Quenching Dynamics in CdSe/ZnS Core/Shell Quantum Dots-Gold Nanoparticle Conjugates in Aqueous Solution. *J. Appl. Phys.*, **2011**, 109, 124310-1-5.

(33) Mondal, N.; Samanta,A. Ultrafast Charge Transfer and Trapping Dynamics in a Colloidal Mixture of Similarly Charged CdTe Quantum Dots and Silver Nanoparticles. *J. Phys. Chem. C*, **2016**, 120, 650-657.

(34) Nikoobakht, B.; Burda, C.; Braun, M.; Hun, M.; El-Sayed, M. A. The Quenching of CdSe Quantum Dots Photoluminescence by Gold Nanoparticles in Solution. *Photochemistry and Photobiology*, **2002**, 75, 591-597.

(35) Zhang, P.; Li, L.; Dong, C.; Qian H.; Ren J. Sizes of water-soluble luminescent quantum

dots measured by fluorescence correlation spectroscopy *Analytica Chimicia Acta*, **2005**, 546, 46-51.

(36) Dong, C.; Huang X.; Ren J. Characterization of Water-soluble Luminescent Quantum Dots by Fluorescence Correlation Spectroscopy. *Ann. N. Y. Acad. Sci.*, 2008, **1130**, 253-261.

(37) de Thomaz, A. A.; Almeida, D. B.; Pelegati, V. B.; Carvalho, H. F.; Cesar, C. L. Measurement of the Hydrodynamic Radius of Quantum Dots by Fluorescence Correlation Spectroscopy Excluding Blinking. *J. Phys. Chem. C*, **2015**, 119, 4294-4299.

(38) Meldal, M.; Tornøe, C. W. Cu-Catalyzed Azide-Alkyne Cycloaddition. *Chem. Rev.*, **2008**, 108, 2952-3015.

(39) Huisgen, R. Kinetics and Reaction Mechanisms: Selected Examples from Experience of Forty Years. *Pure Appl. Chem.*, **1989**, 61(4), 613-628.

(40) Boisselier, E.; Salmon, L.; Ruiz, J.; Astruc, D. How to very efficiently functionalize gold nanoparticles by click chemistry *Chem.Comm.*, **2008**, 44 , 5788-5790.

(41) Fischler, M; Sologubenko, A.; Mayer, J.; Clever, G.; Burley, G.; Gierlich, J.; Carell, T.; Simon, U. Chain-like assembly of gold nanoparticles on artificial DNA templates via click chemistry. *Chem. Rev.*, **2008**, 2, 169-171.

(42) Zhou, Y.; Wang, S.; Zhang, K., Jiang, X. Visual Detection of Copper(II) by Azide- and Alkyne-Functionalized Gold Nanoparticles Using Click Chemistry. Angew. Chem. Int. Ed., 2008, 47, 7454.

(43) Zhou, Y.; Ma, Z. A novel fluorescence enhanced route to detect copper(II) by click chemistry-catalyzed connection of Au@SiO2 and carbon dots. *Sensors and Actuators B*, **2016**, 233, 426-430.

(44) Schaefer, D. W. Dynamics of Number fluctuations: Motile Microorganisms. *Science*, **1973**, 180, 1293-1295.

(45) "Photon Correlation Spectroscopy and Velocimetry, H. Z. Cummins, E. R. Pike, plenum Press, NY 1977.

(46) Schaerfer, D. W.; Berne, B. J. Light Scattering from Non-Gaussian Concentration Fluctuations. *Phys. Rev. Lett.*, **1972**, 28, 475-478.

(47) N. Thompson, *In* Topics in Fluorescence Spectroscopy; Lakowicz, J. R., Ed.; Plenum Press: New York, 1991; Vol. I.

(48) Pusey, P. N. Number Fluctuation of Interacting Particles. *J. Phys. A*, **1979**, 12, 1805-1818.

(49) Rigler, R.; Mets, Ü. .; Widengren, J. Fluorescence Correlation Spectroscopy with High Count Rate and Low Background: Analysis of Translational Diffusion. *Eur. BioPhys. J*, **1993**, 22, 169-175.

(50) Wang,J-C. Design and Testing of a Novel Microscopic Photon Correlation Spectrometer with Higher Accuracy *J. Opt. A: Pure Appl. Opt.*, **2001**, 3, 360-365.

(51) Barbara, A.; Lopez-Rios, T.; Dumont, S.; Gay, F.; Quémerais, P. Microscope Spectrometer for Light Scattering Investigations. *App. Opt.*, **2010**, 49, 4193-4201.

(52) Einstein, A. On the Movement of Small Particules Suspended in Stationary Liquids Required by the Molecular-Kinetic Theory of Heat. *Ann. d. Phys.*, **1905**, 17, 549-560.

(53) Adamczyk, Z.; Sadlej, K.;Wajnryb, E.; Ekiel-Jezewska, M. L.; Warszyński, P. Hydrodynamic Radii and Diffusion Coefficients of Particle Aggregates Derived from the Bead Model. *J. Colloid Interface Sci.*, **2010**, 347, 192-201.

(54) García de la Torre, J.; del Rio Echenique G.; Ortega, A. Improved Calculation of Rotational Diffusion and Interinsic Viscosity of Bead Models for Macromolecules and Nanoparticles. *J. Phys. Chem.* B, **2007**, 111, 955-961.

(55) Kätzel, U.; Vorbau, M.; Stintz, M.; Gottschalk-Gaudig, T.; Barthel, H. Dynamic Light Scattering for the Characterization of Polydisperse Fractal Systems: II.Relation between Structure and DLS Results. *Part. Part. Syst. Charact.*, **2008**, 25, 19-30.

(56) Barbara, A.; Dubois, F. Ibanez, A. Eng, L. M.; Quémerais, P. SERS Correlation Spectroscopy of Silver Aggregates in Colloidal Suspension: Quantitative Sizing Down to a Single Nanoparticle. *J. Phys. Chem. C*, **2014**, 118, 17922-17931.

(57) Schönweiz, S.; Knoll, S.; Anjass, M.; Braumüller, M.; Rau, S.; Streb, C. "CLICKable" Azide-Functionalized Phosphonates for the Surface-Modification of Molecular and Solid-State Metal Oxides. *Dalton Trans.* **2016**, 45, 1612116124.

(58) Zylstra, J.; Amey, J.; Miska, N. J.; Pang, L.; Hine, C. R.; Langer, J.; Doyle, R. P.; Maye, M. M. A Modular Phase Transfer and Ligand Exchange Protocol for Quantum Dots. *Langmuir*, **2011**, 27, 43714379.

(59) Jasieniak, J.; Smith, L.; van Embden, J.; Mulvaney, P.; Califano, M. Re-examination of the Size-Dependent Absorption Properties of CdSe Quantum Dots. *J. Phys. Chem. C*, **2009**, 113 (45), 19468 19474.

(60) Marti, A.; Costero, A. M.;Gavina, P.; Parra, M. Selective Colorimetric NO(g) Detection with Modified Gold Nanoparticles using Click Chemistry. *Chem. Commun.*, **2015**, 51, 3077-3079.

(61) Hua, C.; Zhang, W. H.; De Almeida, S. R. M.; Ciampi, S.; Gloria, D.; Liu, G.; Harper, J. B.; Gooding, J. J. A novel route to copper(II) detection using click chemistry-induced aggregation of gold nanoparticles. *Analyst*, **2012**, 137, 82-86.

(62) Koppel D.E. Analysis of Macromolecular Polydispersity in Intensity Correlation Spectroscopy: The Method of Cumulants *J. Chem. Phys.*, **1972**, 57, 4814-4820.

(63) Rüttinger S., *Dissertation, Technical University Berlin*, 2007 Confocal Microscopy and Quantitative Single Molecule Techniques for Metrology in Molecular Medicine"

(64) C. F. Bohren, D. R. Huffman, *Absorption and Scattering of Light by Small Particles*, Wiley Science 1998.

(65) Efros, A. L.; Nesbitt, D. J. Origin and control of blinking in quantum dots. *Nature Nanotechnology*, **2016**, 11, 661-671.

(66) Yoo, B. K.; Joo, S-W. *In situ* Raman monitoring triazole formation from self-assembled monolayers of 1,4-diethynylbenzene on Ag and Au surfaces via "click" cyclization. *J. of Colloidal and Interface Science*, **2007**, 311, 491-496.

(67) Sharp, D. B.; Shawcross, A.; Greated, C. A. LIF Measurement of the Diluting Effect of Surface Waves on Turbulent Buoyant Plumes. *J. Flow Control, Measurements & Visualization*, **2014**, 2, 77-93.